

# Histology to $\mu$ CT Data Matching using Landmarks and a Density Biased RANSAC

Natalia Chicherova, Ketut Fundana, Bert Müller and Philippe Cattin

Medical Image Analysis Center, University of Basel  
[natalia.chicherova@unibas.ch](mailto:natalia.chicherova@unibas.ch)

**Abstract.** The fusion of information from different medical imaging techniques plays an important role in data analysis. Despite the many proposed registration algorithms the problem of registering 2D histological images to 3D CT or MR imaging data is still largely unsolved.

In this paper we propose a computationally efficient fully-automatic approach to register 2D histological images to 3D micro Computed Tomography data. The landmark-based approach in combination with a density-driven RANSAC plane-fitting allows efficient localization of the histology images in the 3D data within less than 4 minutes (single-threaded MATLAB code) with an average accuracy of 0.25 mm. The error for mismatched slices equals 2.21 mm. The approach managed to successfully localize 75% of the histology images in our database. The proposed approach is an important step towards solving the problem of registering 2D histology sections to 3D data fully-automatically.

## 1 Introduction

Image-registration is the art of automatically aligning or warping medical imaging data. Registered data allows more in depth analysis of the probed tissues as different modalities often represent different physical properties important to better understand and interpret the data at hand. Many approaches have been proposed in the last decades for 2D-to-2D and 3D-to-3D registration of the same or even different modalities [11]. However, registering 2D histological images to 3D data is a largely unexplored problem.

The need for good 2D histology to 3D data registration becomes more and more important with the availability of affordable micro Computed Tomography ( $\mu$ CT) devices with high spatial resolution and tissue contrast. Combining the functional information from histology with the structural imaging data of the  $\mu$ CT provides better insights in identifying the different tissues.

Only few papers are insofar directly related to the research at hand as they describe the registration of histological sections to CT and MR data. Seise *et al.* [10] proposed an interactive registration of histological sections to CT in the context of radiofrequency ablation. However, apart from not being fully automatic, the registration process relies on an intermediate registration via  $\mu$ CT. Sarve *et al.* [9] registered histological images of bone implants with synchrotron

radiation-based  $\mu$ CT data. Although the registration was multi-modal, the authors chose a rigid alignment and optimized the registration parameters with the computationally expensive methods. Other approaches deal with the registration of histological sections with soft tissue such as in the prostate [8] or the human brain [7] where MRI is more useful than CT. An additional factor is that the acquired  $\mu$ CT or  $\mu$ MR imaging data is generally of large size, amounting up to several hundred megabytes of data. However, only very little research has been devoted to efficiently register these type of data sets [6].

Using images of histological cross sections poses additional challenges to the already ill-posed problem of image registration. First, the histology images are susceptible to uneven lighting (vignetting artifact) and different contrasts from staining. Second, the histological sections may suffer from severe non-rigid deformations originating from the cutting process. Moreover, the histological images generally show different contrasts as compared to the  $\mu$ CT or  $\mu$ MR data that must be handled appropriately. Lastly, the potentially non-uniform background of the histological cuts may lead to erroneous results in the registration process.

In this paper we propose a novel approach for automatic registration of 2D histological cross sections to 3D  $\mu$ CT scans. This fully-automatic landmark-based registration approach makes use of the scale- and rotation-invariant feature detector SURF[3] and a novel proposed density-driven RANSAC[4] plane-fitting.

## 2 Method

An illustration of the algorithmic pipeline is depicted in the Figure 1. First, we determine corresponding feature points between the histological image and each image in the CT volumetric data and extract their associated coordinates. Then, based on these coordinates, we build a 3D point cloud, where the third dimension corresponds to the slice number in the CT data. As the distribution of the matched points is higher in the plane that corresponds best to a given histological slice (see center of Fig. 1) the remaining step reduces to a robust plane fitting in a noisy point cloud.

### 2.1 Data acquisition

The sample data used for this study [1] originates from a jaw bone volume augmentation after tooth extraction study. In total 10 clinical patients were included in this study. Biopsies of the jaw bones were taken 4 and 11 months after implantation. The inner diameter of the specimen tubes was around 3 mm and the length was around 12 mm. Micro Computed Tomography ( $\mu$ CT) of the whole specimen was acquired. Then 5 to 9 histological cross-sections through the horizontal plane of the specimen were taken. Each histological slice (thickness 300  $\mu$ m) resulted in an RGB image of size 2592  $\times$  1944 pixels. The  $\mu$ CT data were 8 bit gray-scale 3D matrices with an average data size of 764  $\times$  764  $\times$  700 pixels, where the vertical axis corresponds to the third dimension.

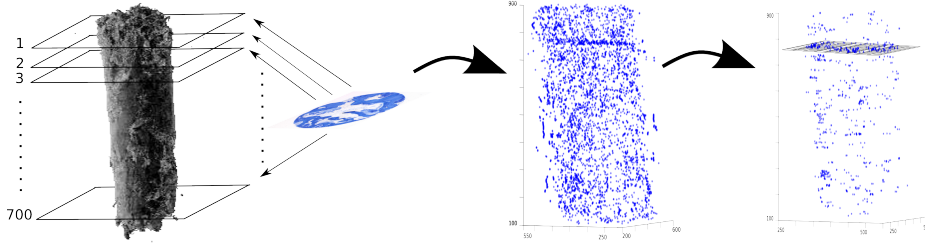


Fig. 1: Pipeline of the algorithm: (left) Feature matching of  $\mu$ CT data and histological image, (middle) 3D point cloud of matched points, (right) optimized RANSAC plane fitting.

## 2.2 Feature detection and matching

Let  $I(x, y)$  and  $V(x, y, z)$  denote the histological image and the  $\mu$ CT data volume, where  $z$  is associated with a slice number in the CT data set where  $I : \Omega_I \subset R^2 \rightarrow R$  and  $V : \Omega_V \subset R^3 \rightarrow R$ . The registration problem between these two modalities can be formulated as finding coefficients of the plane section in the CT space that corresponds best to the histological image. In a first step we match each of the histological images to all axial CT slices using a landmark-based approach. As a feature detection algorithm we rely on the scale- and rotation-invariant feature detector and descriptor SURF [3]. The main principle of this detector is based on scale-space extrema detection and stable feature localization. Applying the feature detector to an image, *e.g.* histological image  $I$ , we obtain a small subset of distinctive feature points  $P(x, y) \subset I$ . The descriptor vectors are then used for matching the feature points between the CT and histological images. For matlab implementation of the algorithm we used an opensource code by D.Kroon saving the default parameters. As the matching algorithm, we use the second-nearest-neighbor-criteria [5,2] that calculates the Euclidean distance between the descriptor vectors. A match is only accepted when the smallest Euclidean distance is less than 0.8 times the second smallest Euclidean distance. This process is then repeated for all the axial slices in the  $\mu$ CT data set.

## 2.3 The 3D feature point cloud

Suppose that the result of the above matching step results in a set of feature points  $P_z \subset V_z$  with coordinates  $(x_i, y_i)$ , where  $i = 1 \dots \kappa$  and  $\kappa$  is the number of found matching feature points in slice  $z$ . Having matched features for each of the  $N$  slices in the CT volume will subsequently allow us to plot them as a point cloud, *i.e.* the 3D set of the keypoints  $C = \{(x_{ij}, y_{ij}, z_j)\}$  ( $j = 1 \dots N$ ) with the third dimension  $z$  representing a slice number in the CT data, see Fig. 1(middle). Here, the total number of feature points for the whole CT data is determined as  $M = \sum_{j=1}^N \kappa_j$ .

As one would expect, the resulting point cloud shows an increased density of found matches at the correct location of the histology section. This holds true even for histological images that are tilted with respect to the  $z$ -axis of the CT data set. This plane - well visible in the point cloud of Fig. 1 - corresponds to the best position for the histological slice. In order to efficiently extract the plane parameters, we define a binary matrix  $B(x, y, z) : \Omega_V \subset R^3 \rightarrow R$  as

$$B(x, y, z) = \begin{cases} 1 & \text{if } (x, y, z) \in C \\ 0 & \text{otherwise,} \end{cases}$$

which is then convolved with a 3D Gaussian as  $B_\sigma = G_\sigma * B$ . Thus, in each point we obtain a new intensity value that is influenced by the neighboring keypoint distribution across the CT space and thus reflects the local density of matched points.

## 2.4 Density-driven RANSAC for robust plane fitting

One of the most widely used robust algorithms for extracting shapes from a data set with outliers is RANSAC [4]. The idea of the algorithm is that a minimum number of points is randomly selected that uniquely defines a fitting model and a corresponding shape primitive is constructed. It then counts the number of points that satisfy the distance threshold  $t$  to the obtained candidate model (inliers). If the number of the inliers is the largest, it extracts the model parameters, otherwise it randomly selects another subset. Depending on the ratio of inliers over outliers this process has to be repeated multiple times to assure with a high probability that a solution is found when present. The huge amount of outliers in our problem result in a very large number of iterations required.

In this work we thus propose to bias the random sampling of the RANSAC plane fitting process towards points with high density *i.e.* points that are close to the plane of interest. To optimize the plane detection algorithm the data set  $B_\sigma$  is further reduced to  $\rho < M$  points by retaining features with the largest density values. However, the new data set  $B_\rho \subset B_\sigma$  still contains some outliers due to high similarities within a specimen along the vertical axis.

To further reduce the number of required sampling iterations, we bias the random sampling code towards preferring points with a higher local density. Thus points with a high local density had a higher probability of being selected. Suppose that each density value of the data set  $B_\rho$  is assigned to the weighting vector  $\mathbf{w} = \{w_k\}$ , where  $k = 1 \dots \rho$ . Therefore, instead of using the unbiased classical sampling of the original RANSAC, the probability of picking an element  $b_m \in B_\rho$  is then defined as  $p_m = \frac{w_m}{\sum_i^\rho w_i}$ .

A further optimization is associated with the angle  $\alpha$  between the  $z$ -axis and the plane formed by the currently randomly sampled points from the data set. Based on our observations we restricted this angle to lie between  $-\alpha_{hist} < \alpha < \alpha_{hist}$ . In other words, for every iteration, the 3D coordinates of the sampled points  $\{b_1, b_2, b_3\} \in B_\rho$  are used to calculate the normal of the plane that goes through these points  $\mathbf{n} = (b_2 - b_1) \times (b_3 - b_1)$ . We then find the angle  $\alpha =$

$\arccos \frac{n_z}{\|n\|}$ , such that  $-\alpha_{hist} < \alpha < \alpha_{hist}$ . Therefore, only planes that satisfy this constraints are considered for further procession in RANSAC.

These two modifications allowed to robustly fit a plane to the selected points and obtain its parameters. An example of the point cloud with corresponding plane fit is shown in the figure 1.

Finally, we make a cut through the CT data matrix along the fitted plane. The image in this cut is the result of our algorithm and should be maximally similar to the histological image.

---

**Algorithm 1** 2D-3D matching

---

**Input:** Histological image  $I$  and  $\mu$ CT 3D data set  $V$ , RANSAC threshold  $t=10$ ,  $\rho=1000$ ,  $\alpha_{hist} = \frac{\pi}{8}$   
**Output:** Plane parameters  $Q$

```

Convert  $I$  to gray scale
for all  $V_j$ , ( $j = 1 \dots N$ ) do                                 $\triangleright$  Detect coordinates of matching points
     $(x_i, y_i) = SURF(I, V_j)$ 
    Build 3D set of coordinates  $C = \{(x_{ij}, y_{ij}, z_j)\}$ 
end for
Create a binary 3D matrix  $B(x, y, z)$ 
for  $(x, y, z) \in B$  do
    if  $(x, y, z) \in C$  then
        set  $B(x, y, z)$  to 1
    end if
end for
Convolve with Gaussian:  $B_\sigma = G_\sigma * B$ 
Find  $\rho$  highest values in  $B_\sigma$ 
Define  $B_\rho \subset B_\sigma$ , that is keep  $\rho$  points with the highest values
 $Q = \text{RANSAC}(B_\rho, t, \alpha_{hist}, w)$        $\triangleright$  Fit a plane into  $B_\rho$  using its values as weights  $w$ 
return  $Q$ 

```

---

### 3 Results

Our framework was validated on 10  $\mu$ CT data sets with overall 60 histological cross section images. For each histological slice we obtained four dimensional vector which uniquely describes a plane in a 3D space. To compare automatically found results with manually found locations we estimated the  $z$ -coordinate along the CT volume and the angle between  $z$ -axis and the normal to the plane which represents a cut of the specimen. The  $z$ -coordinate was calculated as a center point of the obtained plane. All manually found matching parameters were obtained from VG studio which provides a four-dimensional vector of the searching plane and automatically computes the center point of the plane,i.e., $z$ -coordinate. We also performed a visual assessment of the automatically found images. In Fig. 2 you can see an example of what we considered a matched automatically found slice in comparison with the manually found and histological

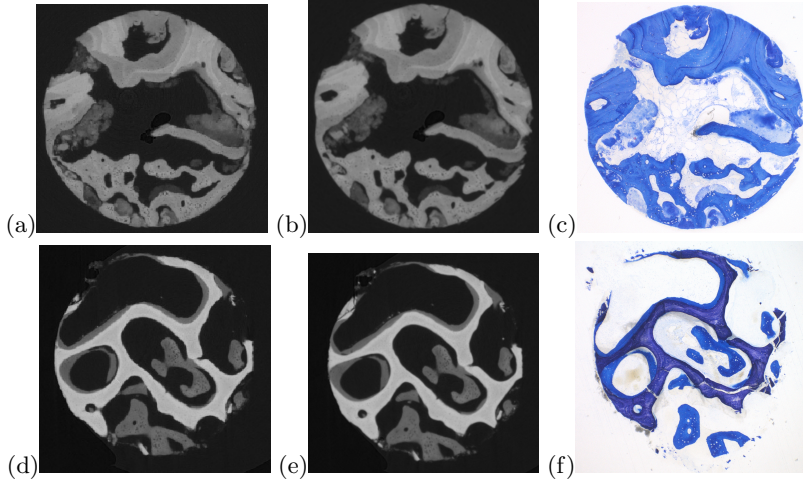


Fig. 2: (a),(d) Automatically found image. (b),(e) Manually found image. (c),(f) Histological image.

image, (a) or (d), (b) or (e) and (c) or (f) accordingly. The complete result of the visual estimation with corresponding comparison with the ground truth values is summarized in table 1. In 9 out of the 10 data sets our approach has allocated at least half of the histological slices with an average difference around 0.25 mm. For the data sets 4, 5 and 10 the algorithm showed poor performance. The average distance for mismatched slices averaged around 286 slices. This might be due to high intensity variations within the CT data set and the inhomogeneous dying of the histological slices (see Fig. 3, (a)). The extrema detector was very sensitive to intensity changes and dirty spots on the histological slices. This caused wrong feature response and consequently incorrectly matched images.

The comparison of the angles with the ground truth is shown in a table 2. For intuitive reasons, we provided negative angles instead of angles around 360 to stress small alternation of the cutting section slopes. For small angles (around 5°) our approach showed high efficiency, whereas, for the angles of more than 10°, which corresponded to 0.53 mm of the specimen, it often found only close approximation to the desired section of the CT volume. For example, for the data set 10, it has found a very close slice number, but determined a wrong angulation.

#### 4 Discussion

Our novel algorithm for automatic 2D-3D registration showed a very high efficiency and small computational complexity and can be readily applied to the matching problem. However, it has certain limitations regarding the feature detection step. Despite the good feature matching performance of SURF for most

Table 1: Number of matched and mismatched images with corresponding average differences between automatically and manually found slices

| Data set                    | 1    | 2    | 3    | 4    | 5    | 6    | 7    | 8    | 9    | 10   |
|-----------------------------|------|------|------|------|------|------|------|------|------|------|
| Number of Matched slices    | 6    | 9    | 6    | 1    | 3    | 5    | 5    | 3    | 3    | 3    |
| Average distance [mm]       | 0.06 | 0.04 | 0.9  | 0.17 | 0.05 | 0.59 | 0.24 | 0.07 | 0.16 | 0.13 |
| Average difference [slices] | 10   | 3    | 8    | 6    | 3    | 63   | 10   | 4    | 10   | 9    |
| Number of Mismatched slices | 0    | 0    | 1    | 4    | 3    | 1    | 1    | 1    | 2    | 3    |
| Average distance [mm]       | -    | -    | 0.17 | 2.71 | 4.56 | 2.96 | 1.07 | 0.67 | 0.76 | 1.37 |
| Average distance [slices]   | -    | -    | 15   | 94   | 286  | 314  | 45   | 40   | 47   | 91   |

Table 2: Comparison of average automatically found angles for matched slices with manually found angles

| Data set                    | 1  | 2  | 3 | 4   | 5 | 6   | 7  | 8  | 9  | 10  |
|-----------------------------|----|----|---|-----|---|-----|----|----|----|-----|
| Average automatic angle [°] | 1  | 1  | 1 | -23 | 4 | -1  | -4 | 5  | 5  | 19  |
| Manual angles [°]           | -2 | -5 | 5 | -22 | 4 | -19 | -7 | 19 | -8 | -13 |

images it can not be considered a multi-modal approach but rather one that is robust against lightning changes. This also explains its poor performance when matching histological sections with non-uniform intensity variations. Moreover, additional complication arose from the histological slices that were compiled from disintegrated pieces (see Fig. 3, (b)) and could not be readily matched with the same specimen. To overcome these limitations we want, first, to focus on developing a feature detector and descriptor that better will account for these specific characteristics and will efficiently work for multi-modal 2D-3D registration. Secondly, we want to include a non-rigid deformation estimation once the initial plane has been found. Lastly, we plan on further speeding up the calculation time by parallelization and GPU implementations. With a computation time of less than 4 min on a single-threaded MATLAB implementation, the algorithm still leaves room for further optimization and parallelization. This irrespective of any angulation between the histology sections with respect to the CT data.

## 5 Acknowledgements

The experimental data were collected and analyzed by Biomaterials Science Center (University of Basel). I would like to thank Stalder, A. K. for the manually found results. The work is supported by SNSF (project 150164).

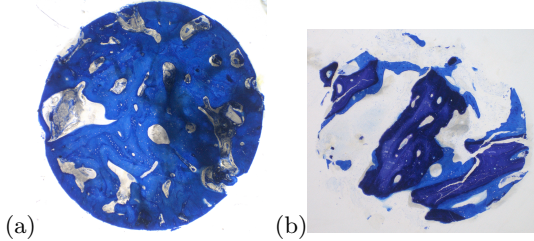


Fig. 3: (a) Inhomogeneous dying of the histological slice from the 16th data set.  
 (b) Compiled from pieces histological slice from the 18th data set.

## References

1. Baumberg, A.: Reliable feature matching across widely separated views. In: Computer Vision and Pattern Recognition, 2000. Proceedings. IEEE Conference on. vol. 1, pp. 774–781. IEEE (2000)
2. Bay, H., Ess, A., Tuytelaars, T., Van Gool, L.: Speeded-up robust features (SURF). Computer vision and image understanding 110(3), 346–359 (2008)
3. Fischler, M.A., Bolles, R.C.: Random sample consensus: a paradigm for model fitting with applications to image analysis and automated cartography. Communications of the ACM 24(6), 381–395 (1981)
4. Lowe, D.G.: Distinctive image features from scale-invariant keypoints. International journal of computer vision 60(2), 91–110 (2004)
5. Mosaliganti, K., Pan, T., Sharp, R., Ridgway, R., Iyengar, S., Gulacy, A., Wenzel, P., de Bruin, A., Machiraju, R., Huang, K., et al.: Registration and 3D visualization of large microscopy images. In: Proc. of SPIE Vol. vol. 6144, pp. 61442V–1 (2006)
6. Osechinskiy, S., Kruggel, F.: Slice-to-volume nonrigid registration of histological sections to MR images of the human brain. Anatomy research international 2011 (2010)
7. Ou, Y., Shen, D., Feldman, M., Tomaszewski, J., Davatzikos, C.: Non-rigid registration between histological and MR images of the prostate: A joint segmentation and registration framework. In: Computer Vision and Pattern Recognition Workshops, 2009. CVPR Workshops 2009. IEEE Computer Society Conference on. pp. 125–132. IEEE (2009)
8. Sarve, H., Lindblad, J., Johansson, C.B.: Registration of 2D histological images of bone implants with 3D SR $\mu$ CT volumes. In: Advances in Visual Computing, pp. 1071–1080. Springer (2008)
9. Seise, M., Alhonnoro, T., Kolesnik, M.: Interactive registration of 2D histology and 3D CT data for assessment of radiofrequency ablation treatment. Journal of pathology informatics 2 (2011)
10. Stalder, A., Ilgenstein, B., Chicherova, N., Deyhle, H., Beckmann, F., Müller, B., Hieber, S.: Combined use of micro computed tomography and histology to evaluate the regenerative capacity of bone grafting materials. International Journal of Materials Research (2013)
11. Zitova, B., Flusser, J.: Image registration methods: a survey. Image and vision computing 21(11), 977–1000 (2003)